Surfaces and Interfaces 23 (2021) 100948

Contents lists available at ScienceDirect

Surfaces and Interfaces

journal homepage: www.sciencedirect.com/journal/surfaces-and-interfaces

Investigation of the Surface Passivation Effect on the Optical Properties of $CsPbBr_3$ Perovskite Quantum Dots

Saif M.H. Qaid [a,b,*], Hamid M. Ghaithan [a], Bandar Ali Al-Asbahi [a,c], Abdullah S. Aldwayyan [a,d,e]

[a] Physics and Astronomy Department, College of Science, King Saud University, Riyadh 11451, Saudi Arabia
[b] Department of Physics, Faculty of Science, Ibb University, Ibb 70270, Yemen
[c] Department of Physics, Faculty of Science, Sana'a University, Yemen
[d] King Abdullah Institute for Nanotechnology, King Saud University, Riyadh 11451, Saudi Arabia
[e] K.A. CARE Energy Research and Innovation Center at Riyadh, Riyadh 11451, Saudi Arabia

ARTICLE INFO

Keywords:
perovskite
$CsPbBr_3$-PQDs
optical parameters
surface passivation

ABSTRACT

The optical properties of inorganic cesium lead bromide perovskite quantum dots ($CsPbBr_3$-PQDs) make them particularly suitable for use as semiconductors. However, surface defects limit the performance of PQDs-based materials and devices. Consequently, this study investigated a surface passivation approach using a special polymer coating under standard conditions. In encapsulation materials, one of the most critical requirements is that the polymer should possess transparency; optical applications require material transparency to avoid affecting optical properties. Additionally, for optical compatibility, a polymer's refractive indices must be significantly different from those of emission materials, and the polymer should be amorphous. Therefore, this study investigated the basic optical properties and parameters of a polymethyl methacrylate polymer-passivated $CsPbBr_3$-PQDs surface and compared them with a bare $CsPbBr_3$-PQDs surface. Optical properties such as absorbance, transmittance, and reflectance are associated with important optical constants, including bandgap, absorption coefficient, extinction coefficient, refractive index, and dielectric constant. With the surface passivation approach, the surface-modification-dependent optical properties of $CsPbBr_3$-PQDs can suppress surface states and improve the surface quality of PQDs-based materials and devices without optical contribution or structural changes. Surface passivation results in enhanced emission, which is key to improving the performance of PQDs-based optoelectronic devices.

1. Introduction

Organic-inorganic (hybrid) and inorganic lead halide perovskite structures with monovalent A cations and X anions (or single and mixed versions) have prominent $APbX_3$ (e.g., A = Cs, MA, and FA; X = Cl, Br, and I). Perovskite and perovskite quantum dots (PQDs) have significant potential for use in optoelectronic applications, including solar cells, photodetectors, and light-emitting devices. Perovskite materials are suitable for such applications on account of their advantageous optoelectronic properties of composition tunability, light absorption and emission over the entire visible spectrum, ultrahigh photoluminescence (PL), quantum yield (QY), narrow emission linewidth, short exciton radiative lifetime, and long carrier diffusion length [1–6].

Inorganic cations (e.g., cesium lead bromide [$CsPbX_3$]) exhibit relatively improved stabilities compared with those of their organic-inorganic hybrid equivalents (e.g., $MAPbX_3$ and $FAPbX_3$). However, the low formation energy of crystal lattices and the high delocalization activity of surface ions makes $CsPbX_3$ very susceptible in practical operation to polar solvents and sensitive to moisture and air, anion-exchange reactions, and thermal heating [7–10]. Such inherent instability significantly impedes the further development and future application of $CsPbX_3$-PQDs in optoelectronics fields. Therefore, it is essential to identify an effective method of improving stability. Several protective strategies have been proposed to enhance the stability of PQDs, including surface passivation. Exposure to external erosive species forms a protective perovskite layer that reinforces the PQDs' stability and other expected properties [8,11–19].

Poor photoelectric efficiency in optical devices results from the presence of surface states typically caused by the recoil of surface bonds and surface contamination; consequently, the passivation of surface

* Corresponding author.
E-mail address: sqaid@ksu.edu.sa (S.M.H. Qaid).

https://doi.org/10.1016/j.surfin.2021.100948
Received 29 September 2020; Received in revised form 6 January 2021; Accepted 13 January 2021
Available online 19 January 2021

states has become an important research focus for practical applications due to the significant effects on the stability and other physical properties of nanoscale materials [20,21]. These superficial features are critical to achieving enhanced performance in optical applications, and surface modifications will result in improved optical responses. Many investigations into surface passivation for traditional semiconductors have been conducted and published [20–26]. For more contemporary materials, such as 2D materials and perovskites, it has been demonstrated that optimizing surface passivation improves these materials and the performance of associated devices. Additionally, various polymers have been introduced into perovskite precursor solutions to control the morphology of perovskite films [27–31]. When used as cooperative additives, some polymers can establish hydrogen bonds with perovskite precursors and promote film growth by acting as 3D templates to enhance the morphology of perovskite films [31]. Surface passivation can involve encapsulation by organic polymer matrices (e.g., polymethyl methacrylate [PMMA] [32,33], polyvinylidene fluoride, ethylene vinyl acetate, or anthracene [34–36]). Furthermore, the surface passivation process can involve encapsulation by some mesoporous inorganic dielectric materials by stuffing PQDs into mesoporous particles via a facile mixing method (e.g., SiO_2 [11,13,16,17,36–39], TiO_2 [19,40,41], or glass sheets [42]). Appropriate processing conditions are essential for ensuring preforms with high optical and mechanical qualities as well as for guaranteeing the compatibility of the polymer films with the perovskite films and solvents with which they will be mixed. Additionally, encapsulation materials should be transparent to ensure optical properties are preserved. This requirement makes polymers with crystalline and semi-crystalline structures less desirable. Moreover, refractive indices in a polymer must differ considerably from the perovskite layer to enable a sizable bandwidth for the periodic reflector [43,44].

Due to mechanical and chemical properties required in encapsulation materials, PMMA polymers have been widely used as a material of choice in plastic optical fiber fabrication [43,45], microfluidics technology [46], and optoelectronic applications [47]. Incorporating noble metal nanoparticles into PMMA controls its optical properties [48], while the metallization of PMMA is used for electrophoresis [47,49] and dielectrophoresis on microfabricated devices [50,51].

Therefore, this study investigates a selection of PMMA to meet all the requirements mentioned above in terms of its optical properties. It uses PMMA as a light-emitting encapsulation material for PQDs on account of its lower crystallinity than homopolymers; consequently, it also has better solubility. Then, the study conducts an in-depth experimental investigation and analysis of the structural and optical effects in $CsPbBr_3$-PQDs for possible surface passivation by PMMA polymers and compares their optical properties and responses to those of a bare $CsPbBr_3$-PQDs surface. A systematic investigation of the optical absorption, transmittance, reflectance, and emission spectra follows along with a calculation of the constant optical parameters to examine the role of surface passivation.

2. Materials and Methods

2.1. Materials

PMMA was purchased from Sigma-Aldrich (Saint Louis, MO, USA) and was used as received without further purification. Powdered $CsPbBr_3$-PQDs was purchased from Quantum Solutions Company (Thuwal, Saudi Arabia) and was prepared by a modified hot injection process. A toluene solution with a purity of 99.8% (Fluka,Buchs, Switzerland) was used to dissolve all the materials.

2.2. Synthesis of $CsPbBr_3$-PQDs thin films

First, the glass substrate was cleaned sequentially in ultrasonic baths with water containing detergent, deionized water, and ethanol, for a period of 15 min in each. Then, 25 mg/mL of the $CsPbBr_3$-PQDs powder was dissolved in a non-polar solvent of toluene and left overnight to enable suitable dispersion and complete dissolution. Then, toluene solutions containing PMMA (50 mg/ml) were prepared as stock solutions by was stirred at 80 °C until the powder was completely dissolved. and it was left at room temperature for cooling to complete the PMMA solution. In this preparation, the thin films were prepared using combined spin coating and drop-casting procedures. A quantity of 50 μL of $CsPbBr_3$-PQDs was dropped onto the clean glass substrate; this was placed in the spin-coating machine (4,000 rpm for 30 s) to prepare homogenous thin films. Then, the films were vacuum dried for 1 h without annealing. Next, 50 μL of PMMA was drop-casted onto the $CsPbBr_3$-PQDs films, to complete the glass/$CsPbBr_3$-PQDs/PMMA film preparation.

2.3. Film characteristics

All measurements were recorded at room temperature in the ambient environment. The structural properties of the developed films were characterized using a transmission electron microscope (TEM) (JEM-1011, JEOL, Tokyo, Japan) at an acceleration voltage of 200 kV. For the TEM characterization, the $CsPbBr_3$ QDs powders were prepared by dilution of 10 μL from QDs solution with 2 mL of hexane followed by placing several drops of a dilute QDs solution onto a carbon-coated copper grid. The crystal phases of the $CsPbBr_3$-PQDs films were characterized by X-ray diffraction (XRD). XRD was performed on an X-ray diffraction system (Miniflex 600, Rigaku, Japan) with copper K_α radiation ($\lambda = 1.5418$ Å); the scanning angle (2θ) varied between 10°–80° at a scanning rate (step size) of 0.02° at $3^\circ/\text{min}^{-1}$. For optical characterization, the $CsPbBr_3$-PQDs was dispersed onto a microscopic glass substrate following the preparation of the solution from perovskite powder. The absorption spectra of the samples were recorded by an ultraviolet-visible (UV–vis) spectrophotometer (V-670, JASCO, Japan). The PL spectra of the perovskite films were obtained using a fluorescence spectrophotometer (FP-8200, JASCO, Japan) in the wavelength range of 350~800 nm. The spectral dependencies of the transmittance and reflectance of the film were obtained using a UV-vis near-infrared spectrophotometer (Cary 5000, Varian, Australia).

3. Results

3.1. Structural characteristics

Figure 1 shows the TEM image and XRD patterns of the prepared samples. The smaller $CsPbBr_3$-PQDs (with a crystallite size of ~6 nm) are presented in Figure 1 (a). The effects of the polymeric surface passivated on the crystal structure of perovskite films are investigated by XRD patterns; therefore, the XRD patterns of the modified $CsPbBr_3$-PQDs surface and the bare $CsPbBr_3$-PQDs surface films are presented and compared in Figure 1 (b). The XRD patterns demonstrate similar features with peaks at $2\theta = 15.33^\circ$, 21.70°, 30.87°, 34.45°, 37.90°, and 43.93° corresponding, respectively, to diffractions from the (100), (110), (200), (210), (211), and (220) planes. The cubic phase at room temperature (RT) can be attributed to the high reaction temperature, and the XRD patterns are consistent with the results of previous work[52]. The appearance of both the (200) plane and the secondary diffraction peak of the (100) plane suggest a crystalline high-purity cubic phase without any defects, which is consistent with the findings of other reports [17, 52–54]. The XRD patterns show similar features for both samples, and the XRD patterns of the sample with the PMMA-passivated $CsPbBr_3$-PQDs surface do not demonstrate any peaks associated with the PMMA polymer. Furthermore, no peak shifts in the XRD patterns are observed, which is attributed to the polymers not being highly absorbent to X-rays, as evidenced in the previous report [1,55]. This indicates that the polymer modifications have no effect on the crystalline structure of the $CsPbBr_3$-PQDs films [30]. Consequently, due to encapsulation, the

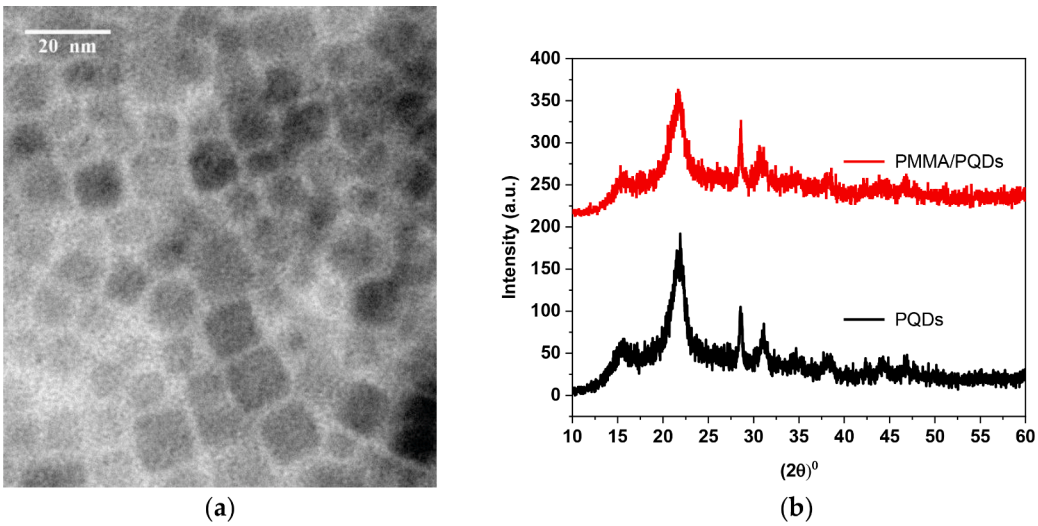

Figure 1. (a) TEM images of the $CsPbBr_3$-PQDs sample. The scale bars in the TEM image correspond to 20 nm. (b) XRD patterns of the PMMA-modified $CsPbBr_3$-PQDs surface and the bare $CsPbBr_3$-PQDs surface thin films.

polymers with crystalline and semi-crystalline structures are less desirable. It can be seen that the PMMA-polymer-passivated $CsPbBr_3$-PQDs surface film shows comparative XRD intensity, and no other phases appear. However, there is no modification by the PMMA-polymer-passivated $CsPbBr_3$-PQDs surface film in the QDs' shape or size (Table 1). From the XRD spectrum, the diameter of the crystallite size (D), the dislocation density (δ), and the micro-strain (ε) in the film can be estimated using the following formulas[4]:

$$D = \frac{K}{\beta\cos\theta}, \ \delta = \frac{1}{D^2} \ and \ \varepsilon \ = \beta\cos\theta \Big/ 4$$

Where k is the shape factor which has a typical value about 0.9, λ is the wavelength of the incident X-ray source, β is the full width at half maximum (FWHM) in radians, and θ is the Bragg's angle. The dislocation density (δ) and the number of crystallites per unit area (N) have been estimated using the following relationship [43–46]. It is observed that the $CsPbBr_3$-PQDs film has grain size of 6.2 nm, which is consistent with the measurements obtained from TEM analyses (Figure 1 [a]). Table 1 summarizes the structural parameters for both samples.

3.2. Optical properties

Optical properties help to categorize the nature of the material using electron movement between different energy levels. Essential optical parameters can be established from measurements of optical reflectivity, transmission, and refraction. Furthermore, the absorption spectrum provides a method to determine the details of a material's existing band states, while the efficiency of electron–hole recombination and information on charge-carrier trapping can be generated from the PL spectrum. Here, to explore the role of surface-passivated PMMA polymers, the optical properties and the parameters of the studied PMMA-polymer-modified $CsPbBr_3$-PQDs surface and the bare $CsPbBr_3$-PQDs surface samples as thin films in the visible regions are presented and compared in detail. The optical parameters for both samples are summarized in Table 2 and demonstrate good correspondence of the $CsPbBr_3$-PQDs polymer in terms of optical properties.

The PL and absorption spectra of the PMMA-modified $CsPbBr_3$-PQDs surface and the bare $CsPbBr_3$-PQDs surface films are presented in Figure 2 and Figure 3 (a). In Figure 2, the modified $CsPbBr_3$-PQDs surface and the bare $CsPbBr_3$-PQDs surface exhibit sharp PL peaks at 515 and 516 nm with narrow FWHMs of 17.5 and 18.4 nm, respectively. The PMMA-polymer-passivated $CsPbBr_3$-PQDs surface films demonstrate significantly increased PLQYs compared with the bare $CsPbBr_3$-PQDs surface, which is attributed to the surface passivation effect of the PMMA coating. This increase indicates a reduction in the amount of non-radiative recombination sites on the surface due to the effective passivation of surface trap states; subsequently, this leads to a reduction in deep traps from the density of state measurement. It is confirmed that the PMMA-polymer-passivated $CsPbBr_3$-PQDs surface film shows changes in both absorption and PL intensity, with reduced absorption intensity and a significant increase in PL intensity. From this study's developed perovskite thin films, it can be assumed that the passivation of surface defects is beneficial to the achievement of amplified spontaneous emission (ASE). The absorption edge and PL peak positions before and after surface passivation confirm a blue shift with the passivated surface, a reduced Stokes shift, and increased PLQY.

It can be seen in Figure 3 (a) that both samples have optical absorption onset that is broad, highly absorbent, and sharp. Furthermore, a decreasing trend with increasing wavelength is evident. Maximum absorption peaks are evident at 350 nm with shoulders at around 508 and

Table 1
Structural properties of the PMMA-modified $CsPbBr_3$-PQDs surface and the unmodified $CsPbBr_3$-PQDs surface thin films at the (110) plane.

$CsPbBr_3$-PQDs	Full width half maximum (FWHM) (deg.)	D (nm)	lattice strain ε× 10^{-3}	Dislocation density δ× 10^{-2} $(nm)^{-2}$
Modified surface	1.570	5.15	6.72	3.77
Unmodified surface	1.427	5.67	6.11	3.11

Table 2
Optical constants of the PMMA-modified $CsPbBr_3$-PQDs surface and the bare $CsPbBr_3$-PQDs surface thin films, respectively, at λ = 410 nm (3.02 eV).

Optical parameter	modified surface	unmodified surface
$\lambda_{ABS}(nm)$	502	500
$\alpha(cm^{-1})$	0.66×10^5	1.91×10^5
$\delta_p(nm)$	151.52	52.36
$E_g(eV)$	2.39	2.40
$B_s(cm^{-2}eV)$	0.62×10^{11}	1.37×10^{12}
K	0.22	0.63
n	1.60	1.51
ε_r	2.51	1.91
ε_i	0.69	1.88
$\sigma(fs)^{-1}$	0.25	0.69
PL Peak	515	516

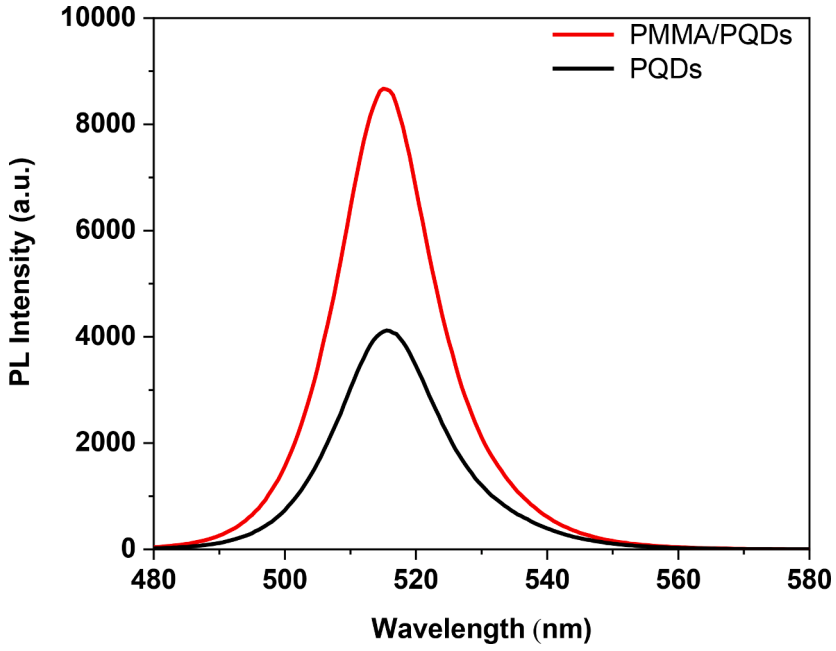

Figure 2. PL spectra of the PMMA-modified-$CsPbBr_3$-PQDs surface and the bare $CsPbBr_3$-PQDs surface thin films.

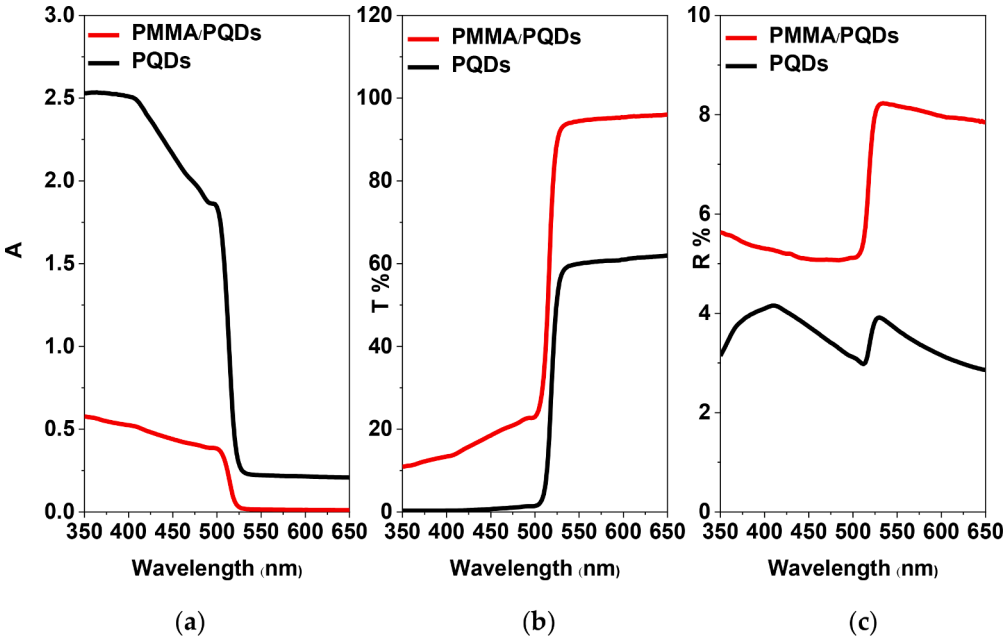

Figure 3. (a) Absorption, (b) transmittance, and (c) reflectance spectra of the PMMA-modified $CsPbBr_3$-PQDs surface and the bare $CsPbBr_3$-PQDs surface thin films.

510 nm for modified and unmodified $CsPbBr_3$-PQDs surface films, respectively. The film on the PMMA-passivated polymer surface tends to possess low absorption, although the passivated surface seems to have a higher coverage; when comparing PMMA to air in the case of the non-passivated surface, this is attributed to the difference in coverage transparency and the reflectivity of the PMMA polymer. The absorption enhancements at the band edge are caused by resonant exciton creation, which provides a plausible explanation for an initially steep rise of the absorption coefficient [56]. The slight blue shift in the absorption onset is attributed to an interaction between the conduction bands with impurity states of higher energy, while the PL shift is attributed to the quantum confinement effect.

In thin-film research, the absorption coefficient (α), extinction coefficient (k), refractive index (n), dielectric constant (ε), and optical conductivity (σ_{opt}) are key parameters. The term n + ik is known as the complex refractive index (N). The dielectric constant is determined after establishing both the refractive index and the absorption coefficient, and all the above parameters are determined using spectral data. While α indicates how much light is absorbed by a material of a given thickness (d), k indicates the absorption loss when the electromagnetic wave propagates through the material [57]. The transmittance (T) and reflectance (R) spectra of PMMA modified and unmodified $CsPbBr_3$-PQDs surface films deposited onto a transparent glass substrate (in the case of air/film/substrate/air configuration at normal incidence) from thin layers of perovskite must first be obtained to calculate the absorption coefficient (α).

Figures 3 (b) and (c) present the optical transmittance (T) and reflectance (R) spectra with and without PMMA coating, respectively, in the visible range for $CsPbBr_3$-PQDs films with a thickness of 300 nm (measured by a surface profilometer). When the wavelength is less than 517 nm (2.40 eV), high absorption is evident. The transmittance of the films is less than 20% and increases almost linearly from 2% for the modified $CsPbBr_3$-PQDs surface and the bare $CsPbBr_3$-PQDs surfaces, respectively. A sharp edge at ~517 nm is visible, with a slight decrease in absorption and a rapid increase in transmittance near to 90% and above 60% for the modified $CsPbBr_3$-PQDs surface and the bare $CsPbBr_3$-PQDs surfaces, respectively. For the 300 nm thick film at ~650 nm, the highest transmissions are at 95% and 62% for the modified $CsPbBr_3$-PQDs surface and the bare $CsPbBr_3$-PQDs surface, respectively. At photon energies below the steep rise in absorption onset at 2.40 eV, the transmission and reflectance spectra exhibit clear thin-film interference (Fabry−Perot effects). This indicates a uniform film thickness and an optically flat surface, preventing any substantial light scattering [56]. The $CsPbBr_3$-PQDs films reveal transmittance spectra in different spectral zones in terms of the change in the absorption coefficient value between high, low, and transparent regions ($\alpha = 0$). Different behavior is evident in the absorption and permeability spectra, and the absorption and α values start to reduce transmission until reaching the region of strong absorption; here, transmission decreases dramatically, almost exclusively due to the influence of α. The region of strong absorption is characterized by interference-free transmittance and reflectance spectra.

The data in Figure 3 (a) was used to calculate the absorption coefficient shown in Figure 4, the refractive index, and the extinction coefficient for a film thickness of d = 300 nm, as shown in Figures 5 (a) and (b). The value for α can be calculated from independently measured T and R data using the approximated relation [58] of $\alpha = \frac{1}{d}\ln\left(\frac{1-R}{T}\right)$, where d is the film thickness for the air/film/substrate/air configuration. The relation (1−R)/T completely eliminates residual oscillations from the optical interference effect when α is calculated [58]. Figure 4 (a) demonstrates the dependence of the absorption coefficient α(λ) with photon energy (hv) for both films calculated from T and R data. At λ = 350 nm, the absorption coefficients are 0.45×10^5 cm^{-1} and 1.95×10^5 cm^{-1} for the modified $CsPbBr_3$-PQDs surface and the bare $CsPbBr_3$-PQDs surface, respectively, which corresponds with respective penetration depth values of 222 and 51 nm. This is less evident in the visible light wavelength range α(λ) of the modified $CsPbBr_3$-PQDs surface than for the bare $CsPbBr_3$-PQDs surface. Based on these results and on account of high absorption coefficient values and shorter corresponding penetration depths, thin layers of both PQDs films can be used in optoelectronic devices to enhance charge collection at the electrodes. These absorption coefficient results provide the potential to exploit the full features of the energy of the photons that is greater than the bandgap of the PQDs film, which is essential for determining the light-harvesting capacities of the materials [59–63].

The first possible benefits come from calculating the absorption coefficient to establish the nature of optical transitions. Information concerning bandgap can be obtained by studying the fundamental absorption edge, and the optical absorption edge can be analyzed using the Tauc relationship [2,64–67], as follows:

$$(\alpha h\nu)^n = B_s\left(h\nu - E_g\right), \quad (1)$$

where A is a constant, E_g is the bandgap, and the values for n are 2 and 1/2 for direct and indirect transitions, respectively.

From a Tauc analysis, the optical absorbance data for the sample in question that spans a range of energies from below the band-gap transition to above it can be acquired. Plotting the $(\alpha h\nu)^n$ versus (hν) is a matter of determining n = 2 or n = 1/2 to compare which provides the better fit and thus identifies the correct transition type. From the diagrams of $(\alpha h\nu)^{1/2}$ vs. (hν) (Figure 5) and $(\alpha h\nu)^2$ vs. (hν) (Figure 6) for the modified $CsPbBr_3$-PQDs surface and the bare $CsPbBr_3$-PQD surface thin films shown in Figure 4, the plot is observed to be linear over a wide range of photon energies and the curve intercepts the X-axis for n=2 and the opposite can found for n=1/2 (no intercept with the X-axis at α=0), which indicates a direct type of transition. This linear region has been used to extrapolate to the X-axis intercept to find the bandgap value. At even higher energies, the absorption processes saturate and the curve again deviates from linear. The energy band gaps can be determined from the intercepts of these plots (straight lines) at zero absorption on the energy axis, which reflect the energy band gaps at these points. By comparing the modified $CsPbBr_3$-PQDs surface and the bare $CsPbBr_3$-PQDs surface thin films, respectively, the optical band gap E_g is found at the beginning of the interband absorption and can be defined as the edge centered at 2.39 and 2.40 eV. The optical band gap of the PMMA-polymer-passivated $CsPbBr_3$-PQDs surface thin films is 2.39 eV, which is consistent with the bare $CsPbBr_3$-PQDs surface thin films. For a direct

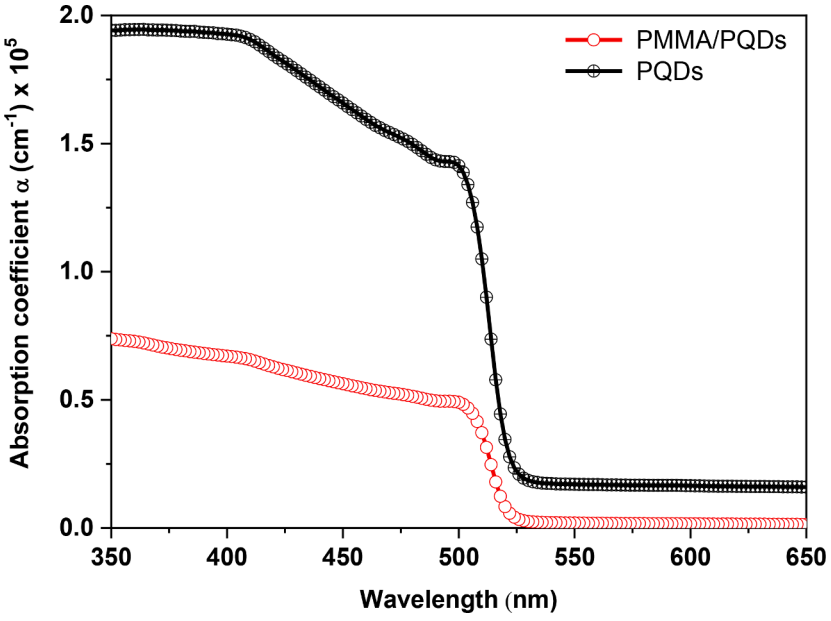

Figure 4. Absorption coefficients curve of the PMMA-modified $CsPbBr_3$-PQDs surface and the bare $CsPbBr_3$-PQDs surface thin films.

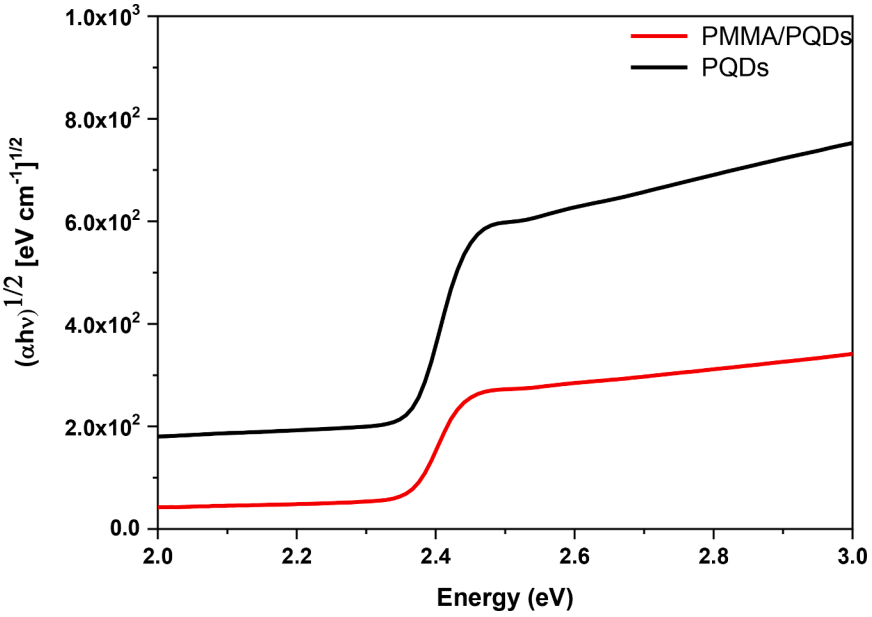

Figure 5. Plots of $(\alpha h\nu)^{1/2}$ vs. E for indirect transitions for the PMMA-modified $CsPbBr_3$-PQDs surface and the bare $CsPbBr_3$-PQDs surface thin films.

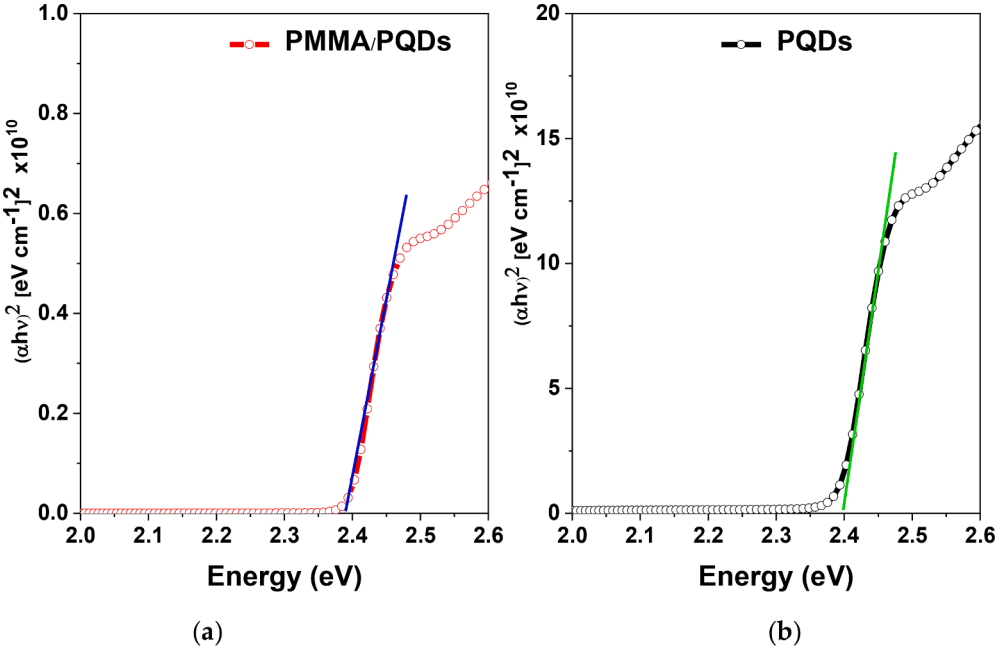

Figure 6. Plots of $(\alpha h\nu)^2$ vs. E for direct transitions for (a) the PMMA-modified $CsPbBr_3$-PQDs surface and (b)the bare $CsPbBr_3$-PQDs surface thin films.

semiconductor and from the Figure 6, the band edge sharpness values (B_s) can also be found through derivation from the slope of the plot of $(\alpha h\nu)^2$ vs. $(h\nu)$ in the absorption of the band-to-band range [66]. The B_s values are 0.62×10^{11} cm^{-2} eV for the modified $CsPbBr_3$-PQDs surface thin films and 1.37×10^{12} cm^{-2} eV for the bare $CsPbBr_3$-PQDs surface thin films. In the visible light wavelength range, the B_s of the modified $CsPbBr_3$-PQDs surface is clearly smaller than that of the bare $CsPbBr_3$-PQDs surface, although both have direct band gaps. From the values of the optical band gap E_g and the sharpness of the band edge B_s, a small difference is observed in the optical band gap, while the band edge sharpens when surface passivation by the PMMA polymer decreases by around one order when compared with the non-passivated surface.

The complex refractive index (N) (in which $N = n + ik$) for the film with a thickness (d), where the real part of the refractive index is n and the imaginary part is k, can be determined using the measured data for both T and R in Figure 3 (a) and the absorption coefficient α(λ) presented in Figure 4. It can be expressed in terms of (α) using Eq. (2)

$$k = \frac{\alpha\lambda}{4\pi} \tag{2}$$

to examine the extinction coefficient k(λ) result in terms of (R) using Eq. (3)

$$\left(n = \frac{(1+\sqrt{R})}{(1-\sqrt{R})}\right) \tag{3}$$

for the refractive index of the layer where light is perpendicular to the planar film [66–68]. The spectral dependencies of the extinction

coefficient k(λ), the refractive index n(λ), and the thin films of the modified $CsPbBr_3$-PQD surface and the bare $CsPbBr_3$-PQDs surface are presented in Figures 7(a) and (b), respectively.

In Figure 7(a), the k(λ) result exhibits absorption peaks located at ≈410 and 517 nm and demonstrates a decreasing trend of k(λ) as λ increases above ~410 nm. The second absorption peak at ≈517 nm is attributed to the transition from the valence band to the conduction band. The k(λ) value increases commensurate with wavelength and follows a linear trend until reaching the peak value at 410 nm for both samples. Then, in the range of 410–510 nm, k(λ) slowly decreases. For the modified $CsPbBr_3$-PQD surface, the k(λ)peaks are close to 0.22 and 0.21, respectively, at the same wavelength position. For the unmodified $CsPbBr_3$-PQDs film, the k(λ) peaks are close to 0.62 and 0.59 at 410 and 510 nm, respectively. Additionally, a sharp decrease in k(λ) is represented by the sharp edge at 517 nm. After the band edge, the values of k (λ) for both samples are almost constant, and the values of k(λ) before the band edge are greater than those in subsequent regions. Figure 7 (b) demonstrates the dependence of the refractive indices on wavelength, while Figure 7 (a) compares the estimated spectral variation of the refractive indices n(λ) in the visible regions for the modified $CsPbBr_3$-PQDs surface and the bare $CsPbBr_3$-PQDs surface thin films. The tendencies of the refractive indices for the modified $CsPbBr_3$-PQDs surface and the bare $CsPbBr_3$-PQDs surface thin films are identified, respectively, as follows: For the bare $CsPbBr_3$-PQDs thin films, one sharp peak with a value of 1.50 is evident at 410 nm, while another slowly changing peak near to 1.49 appears at 517 nm. There is also a small peak at 510 nm. In the region of 350–410 nm, the refractive indices increase from 1.43 to 1.50 then decrease again to 1.42 at 510 nm. There is a sharp increase at the band edge to 1.51, followed by a linear decrease. For the modified $CsPbBr_3$-PQDs thin films, the refractive index is almost constant at around 1.6 from 350 to 510 nm. At the band edge, the refractive index of the films increases up to almost 1.82 before becoming constant, which implies that PMMA is an ideal anti-reflective coating with the potential to be used in ASE efficiency and fiber optics applications. It is clear that as absorbance below the band edge increases, the real part of the complex refractive index (n) exhibits a noticeable decrease with increasing wavelength. This can be explained by the reflectance, which can modify both the refractive index and the film's reflectivity. Generally, the refractive index of the films is approximately 1.58–1.84 for the modified $CsPbBr_3$-PQDs surface and 1.44–1.54 for the bare $CsPbBr_3$-PQDs surface.

In summary, the extinction coefficient (k) of the modified $CsPbBr_3$-PQDs surface sample is smaller than that of the unmodified $CsPbBr_3$-PQDs surface sample, with values of 0.16 and 0.62 at λ = 410 nm, respectively. The (k) representation of the absorption coefficient clearly reveals two edges with onsets at 410 and 517 nm, reflecting the above-mentioned transitions. At λ = 410 nm, the modified $CsPbBr_3$-PQDs surface sample has a higher refractive index (n) than the unmodified $CsPbBr_3$-PQDs sample at 1.59 and 1.51, respectively.

The polarizability of any solid material is proportional to its dielectric constant, which is the ratio of the permittivity of a substance to the permittivity of free space. The relative permittivity of the incidental light onto the optical materials is the key parameter used for determining the real (ε_r) and imaginary (ε_i) dielectrics constants, which together make the complex dielectric constant ε:

$$\varepsilon = \varepsilon_r + i\varepsilon_i, \tag{4}$$

Describing the dielectric constant uses the refractive index and extinction coefficient (k) optical parameters to define the real and imaginary parts of the dielectric constant as functions of n(λ) and k(λ). The real and imaginary parts of the dielectric constant are calculated using equations $\varepsilon_r = n^2 - k^2$ and $\varepsilon_i = 2nk$, as seen in Figures 8 (a) and (b), respectively.

The real and imaginary components of the complex dielectric constants of both films are shown in Figure 8. Like the refractive indices that change with wavelength (Fig. 7 [b]), the real components follow the same pattern. In the region of 350–510 nm, the real components ε_r are almost constant with values of 1.9 and 2.1 before increasing sharply to 2.25 and 3.50 at the band edge for the modified and unmodified $CsPbBr_3$-PQDs surface thin films, respectively. Then, ε_r is almost constant for the modified thin films, while the value follows a linear decrease for the unmodified $CsPbBr_3$-PQDs surface sample. The components follow the same pattern as the extinction coefficient, which changes with wavelength (Fig. 7 [a]). The imaginary component ε_i has peaks at 410 and 510 nm. The real part of the dielectric constant is at 2.60 and 1.58, while at a photon energy of 3.02 eV (410 nm), the

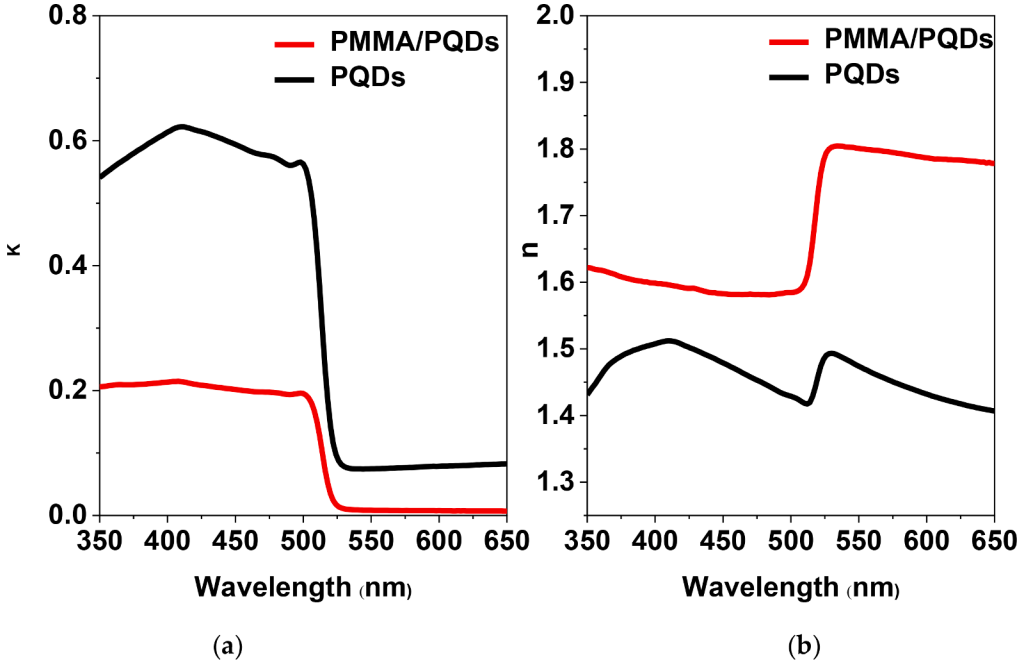

Figure 7. The calculated (a) extinction coefficients k(λ) and (b) refractive index n(λ) curves of the PMMA-modified $CsPbBr_3$-PQDs surface and the bare $CsPbBr_3$-PQDs surface thin films.

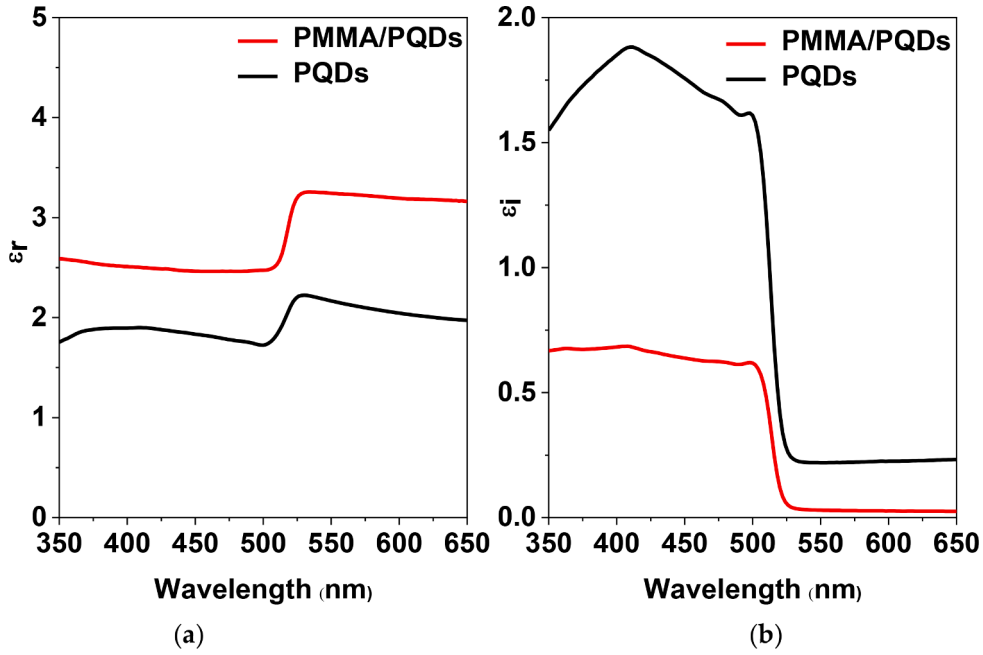

Figure 8. (a) Real components and (b) imaginary components of the complex dielectric constant of the PMMA-modified $CsPbBr_3$-PQDs surface and the bare $CsPbBr_3$-PQDs surface thin films.

imaginary part of the dielectric constant is located at 0.75 and 1.75 for the modified $CsPbBr_3$-PQDs surface and the bare $CsPbBr_3$-PQDs surface thin films, respectively.

It is understood that the amount of energy stored and dissipated in a dielectric due to an applied electric field is related to the real and the imaginary parts of the dielectric constant, respectively [[68]]. The high dielectric constant of active material in light-emitting-based diode devices increases the number of electrons and reduces the number of holes that reach the emission zone by enhancing the electrical field, thereby facilitating the injection of electrons and supporting optical efficiency and brightness in the device. The high dielectric constant also explains the low binding energies of the exciton, since the photoinduced charges can effectively be screened out by the dipoles of the lattice [68–73]. The dielectric constant is related to both the band structure and the optical conductivity. The nature of the optical charge generation and transport within a device can also be determined using photoconductivity (σ_{ph}), which is another optical parameter that can be obtained from the measurement of the absorption coefficient and refractive index via the Eq. (5) [2]:

$$\sigma_{ph} = \frac{nc}{4\pi}, \tag{5}$$

where c is the velocity of light.

Additionally, the high optical conductivity value confirms the suitability of the films for use in photovoltaic applications. Figure 9 contains the optical conductivity with photon energy results for the modified $CsPbBr_3$-PQDs surface and the bare $CsPbBr_3$-PQDs surface thin films.

The optical conductivity of the PMMA-modified $CsPbBr_3$-PQDs

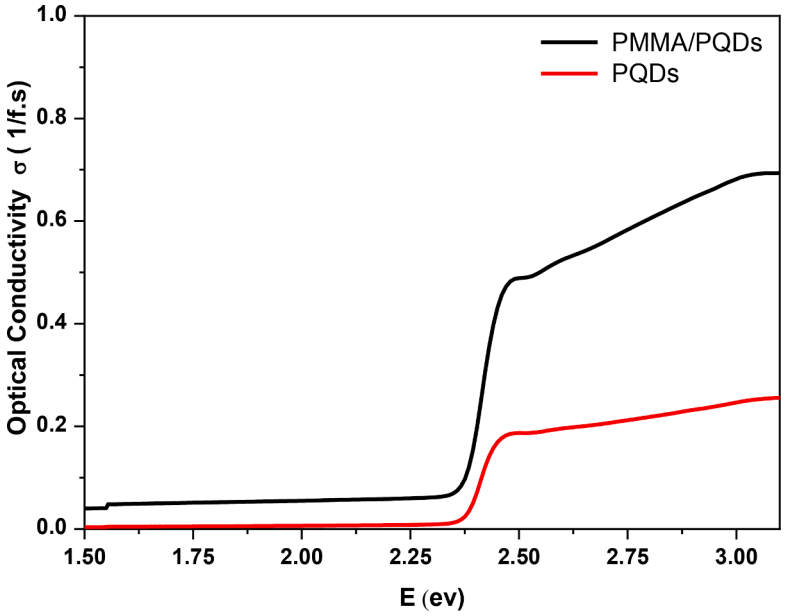

Figure 9. Optical conductivity of the complex dielectric constant of the PMMA-modified $CsPbBr_3$-PQDs surface and the bare $CsPbBr_3$-PQDs surface thin films.

surface sample (0.15 $[fs]^{-1}$) is lower than that of the bare $CsPbBr_3$-PQDs surface sample (0.75 $[fs]^{-1}$) throughout the visible region. This conductivity can depend on two factors: the charge mobility and/or the concentration of the free carriers (carrier densities) by the relationship $\sigma = n_d e \mu_e$, where n_d is the number density of the free electrons and μ_e is the electron mobility [74]. This relationship supports the fact that an increase in the mobility and/or concentration of the free carriers implies an increase in conductivity. Therefore, it can be concluded that even with low carrier densities, high carrier mobilities ensure a significant free carrier contribution to optical conductivity. Consequently, it is expected that charge carrier mobility in the modified $CsPbBr_3$-PQDs surface sample will be smaller, which implies that photocarriers will cross fewer grain boundaries, resulting in fewer crystalline defects.

Finally, the surface passivation approach can suppress surface states and improve the surface quality of PQDs-based materials and devices without affecting either optical or structural properties.

5. Conclusions

In summary, this study performed a comparative investigation of $CsPbBr_3$-PQDs both with and without PMMA surface passivation. The investigation analyzed the effect of surface passivation on the optical parameters and structural properties of $CsPbBr_3$-PQDs and the stability of $CsPbBr_3$-PQDs properties. Additionally, the study determined the real (n) and imaginary (k) parts of the complex refractive index and dielectric constants of the PQDs thin films. The optical band gap (Eg) was established, and the optical absorption spectra reveal the absorption mechanism to be a direct transition. The results show that the modified films possess lower roughness values and better photoelectric properties compared with the reference sample. Furthermore, the surface passivation of the $CsPbBr_3$-PQDs film by the PMMA polymer was found to have a significant impact on the optical properties of $CsPbBr_3$-PQDs materials, and only a small change in the optical parameters results from surface passivation. The PMMA solution in toluene provided an optically transparent layer that was attached to the PQDs layer. The appropriate selection of PMMA and processing conditions is crucial to ensuring the resultant preforms possess high optical and mechanical qualities and the polymer films and perovskite films are compatible. To the best of the authors' knowledge, this is the first publication of an experimental study on the effect of PMMA on $CsPbBr_3$-PQDs. In the $CsPbBr_3$-PQDs film, surface passivation is found to improve PLQY due to fewer deep-trap states of the as-exchanged $CsPbBr_3$-PQDs, while the optical absorption is reduced simultaneously. The surface passivation of $CsPbBr_3$-PQDs is found to be more stable under ambient conditions that promote desirable changes in optical properties; these are beneficial in the production of more stable optoelectronic devices. The findings of this study indicate that surface passivation is useful for achieving both high performance and stability; therefore, optimizing the most effective PMMA thickness is essential.

CRediT authorship contribution statement

Saif M.H. Qaid: Conceptualization, Visualization, Methodology, Investigation, Formal analysis, Data curation, Supervision, Writing - original draft. **Hamid M. Ghaithan:** Investigation, Formal analysis. **Bandar Ali Al-Asbahi:** Validation, Data curation. **Abdullah S. Aldwayyan:** Supervision, Data curation, Validation.

Declaration of Competing Interest

The authors declare that they have no known competing financial interests or personal relationships that could have appeared to influence the work reported in this paper.

Acknowledgments

The authors extend their appreciation to the Deputyship for Research & Innovation, "Ministry of Education" in Saudi Arabia for funding this research work through the project no.(IFKSURG-1440-038).

References

[1] S.M.H. Qaid, B.A. Al-Asbahi, H.M. Ghaithan, M.S. AlSalhi, A.S. Al dwayyan, Optical and structural properties of CsPbBr3 perovskite quantum dots/PFO polymer composite thin films, J. Colloid Interface Sci. 563 (2020) 426–434, https://doi.org/10.1016/j.jcis.2019.12.094.

[2] B.A. Al-Asbahi, S.M.H. Qaid, M. Hezam, I. Bedja, H.M. Ghaithan, A.S. Aldwayyan, Effect of deposition method on the structural and optical properties of CH3NH3PbI3 perovskite thin films, Opt. Mater. (Amst). 103 (2020), 109836, https://doi.org/10.1016/j.optmat.2020.109836.

[3] A. Kojima, K. Teshima, Y. Shirai, T. Miyasaka, Organometal halide perovskites as visible-light sensitizers for photovoltaic cells, J. Am. Chem. Soc. 131 (2009) 6050–6051.

[4] N.K. Kumawat, D. Gupta, D. Kabra, Recent Advances in Metal Halide-Based Perovskite Light-Emitting Diodes, Energy Technol (2017), https://doi.org/10.1002/ente.201700356.

[5] L. Dou, Y.(Micheal) Yang, J. You, Z. Hong, W.-H. Chang, G. Li, Y. Yang, Solution-processed hybrid perovskite photodetectors with high detectivity, Nat. Commun. 5 (2014) 5404, https://doi.org/10.1038/ncomms6404.

[6] S.M.H. Qaid, M.N. Khan, A. Alqasem, M. Hezam, A. Aldwayyan, Restraining effect of film thickness on the behaviour of amplified spontaneous emission from methylammonium lead iodide perovskite, IET Optoelectron 13 (2018) 1–5, https://doi.org/10.1049/iet-opt.2018.5035.

[7] Y. Wei, Z. Cheng, J. Lin, An overview on enhancing the stability of lead halide perovskite quantum dots and their applications in phosphor-converted LEDs, Chem. Soc. Rev. (2019) 48, https://doi.org/10.1039/c8cs00740c.

[8] I. Levchuk, A. Osvet, X. Tang, M. Brandl, J.D. Perea, F. Hoegl, G.J. Matt, R. Hock, M. Batentschuk, C.J. Brabec, Brightly Luminescent and Color-Tunable Formamidinium Lead Halide Perovskite FAPbX3 (X = Cl, Br, I) Colloidal Nanocrystals, Nano Lett 17 (2017), https://doi.org/10.1021/acs.nanolett.6b04781.

[9] W. Yang, F. Gao, Y. Qiu, W. Liu, H. Xu, L. Yang, Y. Liu, CsPbBr3-Quantum-Dots/Polystyrene@Silica Hybrid Microsphere Structures with Significantly Improved Stability for White LEDs, Adv. Opt. Mater. 7 (2019), https://doi.org/10.1002/adom.201900546.

[10] G. Nedelcu, L. Protesescu, S. Yakunin, M.I. Bodnarchuk, M.J. Grotevent, M. V. Kovalenko, Fast Anion-Exchange in Highly Luminescent Nanocrystals of Cesium Lead Halide Perovskites (CsPbX3, X = Cl, Br, I), Nano Lett 15 (2015), https://doi.org/10.1021/acs.nanolett.5b02404.

[11] Z. Liu, Y. Zhang, Y. Fan, Z. Chen, Z. Tang, J. Zhao, Y. Lv, J. Lin, X. Guo, J. Zhang, X. Liu, Toward Highly Luminescent and Stabilized Silica-Coated Perovskite Quantum Dots through Simply Mixing and Stirring under Room Temperature in Air, ACS Appl. Mater. Interfaces. (2018) 10, https://doi.org/10.1021/acsami.7b18964.

[12] C. Sun, Y. Zhang, C. Ruan, C. Yin, X. Wang, Y. Wang, W.W. Yu, Efficient and Stable White LEDs with Silica-Coated Inorganic Perovskite Quantum Dots, Adv. Mater. (2016) 28, https://doi.org/10.1002/adma.201603081.

[13] E. Yassitepe, Z. Yang, O. Voznyy, Y. Kim, G. Walters, J.A. Castañeda, P. Kanjanaboos, M. Yuan, X. Gong, F. Fan, J. Pan, S. Hoogland, R. Comin, O. M. Bakr, L.A. Padilha, A.F. Nogueira, E.H. Sargent, Amine-Free Synthesis of Cesium Lead Halide Perovskite Quantum Dots for Efficient Light-Emitting Diodes, Adv. Funct. Mater. 26 (2016) 8757–8763, https://doi.org/10.1002/adfm.201604580.

[14] M. Meyns, M. Perálvarez, A. Heuer-Jungemann, W. Hertog, M. Ibáñez, R. Nafria, A. Genç, J. Arbiol, M.V. Kovalenko, J. Carreras, A. Cabot, A.G. Kanaras, Polymer-Enhanced Stability of Inorganic Perovskite Nanocrystals and Their Application in Color Conversion LEDs, ACS Appl. Mater. Interfaces. 8 (2016) 19579–19586, https://doi.org/10.1021/acsami.6b02529.

[15] D. Yan, T. Shi, Z. Zang, T. Zhou, Z. Liu, Z. Zhang, J. Du, Y. Leng, X. Tang, Ultrastable CsPbBr 3 Perovskite Quantum Dot and Their Enhanced Amplified Spontaneous Emission by Surface Ligand Modification, Small 15 (2019), 1901173, https://doi.org/10.1002/smll.201901173.

[16] Y. Cai, L. Wang, T. Zhou, P. Zheng, Y. Li, R.J. Xie, Improved stability of CsPbBr3 perovskite quantum dots achieved by suppressing interligand proton transfer and applying a polystyrene coating, Nanoscale 10 (2018), https://doi.org/10.1039/c8nr06607h.

[17] H.C. Yoon, S. Lee, J.K. Song, H. Yang, Y.R. Do, Efficient and Stable CsPbBr 3 Quantum-Dot Powders Passivated and Encapsulated with a Mixed Silicon Nitride and Silicon Oxide Inorganic Polymer Matrix, ACS Appl. Mater. Interfaces. 10 (2018) 11756–11767, https://doi.org/10.1021/acsami.8b01014.

[18] Y. Wang, S. Cao, J. Li, H. Li, X. Yuan, J. Zhao, Improved ultraviolet radiation stability of Mn2+-doped CsPbCl3 nanocrystals: Via B-site Sn doping, CrystEngComm 21 (2019), https://doi.org/10.1039/c9ce01150a.

[19] Z.J. Li, E. Hofman, J. Li, A.H. Davis, C.H. Tung, L.Z. Wu, W. Zheng, Photoelectrochemically active and environmentally stable cspbbr3/tio2 core/shell nanocrystals, Adv. Funct. Mater. 28 (2018), https://doi.org/10.1002/adfm.201704288.

[20] M. Nishida, Energy Distribution of Dangling-Orbital Surface States on the (110) Surface of III-V Compounds, Phys. Status Solidi. 99 (1980), https://doi.org/10.1002/pssb.2220990155.

[21] L. Wang, K. Wu, Q.M. Dong, X.Y. Li, S.Y. Xiong, L.T. Xu, P. Liang, Effect of surface passivation on optical and electronic properties of ultrathin silicon nanosheets, Sci. China Inf. Sci. 55 (2012), https://doi.org/10.1007/s11432-012-4575-x.

[22] H. Tan, A. Jain, O. Voznyy, X. Lan, F.P.G. De Arquer, J.Z. Fan, R. Quintero-Bermudez, M. Yuan, B. Zhang, Y. Zhao, F. Fan, P. Li, L.N. Quan, Y. Zhao, Z.H. Lu, Z. Yang, S. Hoogland, E.H. Sargent, Efficient and stable solution-processed planar perovskite solar cells via contact passivation, Science (80-.) (2017) 355, https://doi.org/10.1126/science.aai9081.

[23] S. Zhu, J. Shao, Y. Song, X. Zhao, J. Du, L. Wang, H. Wang, K. Zhang, J. Zhang, B. Yang, Investigating the surface state of graphene quantum dots, Nanoscale 7 (2015), https://doi.org/10.1039/c5nr01178g.

[24] M. Klaumünzer, J. Hübner, D. Spitzer, C. Kryschi, Surface Functionalization and Electrical Discharge Sensitivity of Passivated Al Nanoparticles, ACS Omega 2 (2017), https://doi.org/10.1021/acsomega.6b00380.

[25] X. Fang, Z. Wei, D. Fang, X. Chu, J. Tang, D. Wang, X. Wang, J. Li, Y. Li, B. Yao, X. Wang, R. Chen, Surface State Passivation and Optical Properties Investigation of GaSb via Nitrogen Plasma Treatment, ACS Omega 3 (2018), https://doi.org/10.1021/acsomega.7b01783.

[26] R. Ludeke, Sb-induced surface states on (100) surfaces of III-V semiconductors, Phys. Rev. Lett. 39 (1977), https://doi.org/10.1103/PhysRevLett.39.1042.

[27] S. Masi, A. Rizzo, F. Aiello, F. Balzano, G. Uccello-Barretta, A. Listorti, G. Gigli, S. Colella, Multiscale morphology design of hybrid halide perovskites through a polymeric template, Nanoscale 7 (2015), https://doi.org/10.1039/c5nr04715c.

[28] C.Y. Chang, C.Y. Chu, Y.C. Huang, C.W. Huang, S.Y. Chang, C.A. Chen, C.Y. Chao, W.F. Su, Tuning perovskite morphology by polymer additive for high efficiency solar cell, ACS Appl. Mater. Interfaces. 7 (2015), https://doi.org/10.1021/acsami.5b00052.

[29] Y. Zhao, J. Wei, H. Li, Y. Yan, W. Zhou, D. Yu, Q. Zhao, A polymer scaffold for self-healing perovskite solar cells, Nat. Commun. 7 (2016), https://doi.org/10.1038/ncomms10228.

[30] Y. Cai, Z. Zhang, Y. Zhou, H. Liu, Q. Qin, X. Lu, X. Gao, L. Shui, S. Wu, J. Liu, Enhancing the efficiency of low-temperature planar perovskite solar cells by modifying the interface between perovskite and hole transport layer with polymers, Electrochim. Acta. 261 (2018), https://doi.org/10.1016/j.electacta.2017.12.135.

[31] X. Di, Z. Hu, J. Jiang, M. He, L. Zhou, W. Xiang, X. Liang, Use of long-term stable CsPbBr3 perovskite quantum dots in phospho-silicate glass for highly efficient white LEDs, Chem. Commun. 53 (2017), https://doi.org/10.1039/c7cc06486a.

[32] L. Protesescu, S. Yakunin, M.I. Bodnarchuk, F. Krieg, R. Caputo, C.H. Hendon, R. X. Yang, A. Walsh, M.V. Kovalenko, Nanocrystals of Cesium Lead Halide Perovskites ($CsPbX_3$, X = Cl, Br, and I): Novel Optoelectronic Materials Showing Bright Emission with Wide Color Gamut, Nano Lett 15 (2015) 3692–3696, https://doi.org/10.1021/nl5048779.

[33] Y. Wang, J. He, H. Chen, J. Chen, R. Zhu, P. Ma, A. Towers, Y. Lin, A.J. Gesquiere, S.T. Wu, Y. Dong, Ultrastable, Highly Luminescent Organic–Inorganic Perovskite–Polymer Composite Films, Adv. Mater. 28 (2016) 10710–10717, https://doi.org/10.1002/adma.201603964.

[34] Q. Zhou, Z. Bai, W.G. Lu, Y. Wang, B. Zou, H. Zhong, In Situ Fabrication of Halide Perovskite Nanocrystal-Embedded Polymer Composite Films with Enhanced Photoluminescence for Display Backlights, Adv. Mater. 28 (2016), https://doi.org/10.1002/adma.201602651.

[35] Y. Li, Y. Lv, Z. Guo, L. Dong, J. Zheng, C. Chai, N. Chen, Y. Lu, C. Chen, One-Step Preparation of Long-Term Stable and Flexible CsPbBr3 Perovskite Quantum Dots/Ethylene Vinyl Acetate Copolymer Composite Films for White Light-Emitting Diodes, ACS Appl. Mater. Interfaces. 10 (2018), https://doi.org/10.1021/acsami.8b02857.

[36] X. Shen, C. Sun, X. Bai, X. Zhang, Y. Wang, Y. Wang, H. Song, W.W. Yu, Efficient and Stable CsPb(Br/I)3@Anthracene Composites for White Light-Emitting Devices, ACS Appl. Mater. Interfaces. 10 (2018), https://doi.org/10.1021/acsami.8b03158.

[37] H. Liao, S. Guo, S. Cao, L. Wang, F. Gao, Z. Yang, J. Zheng, W. Yang, A General Strategy for In Situ Growth of All-Inorganic CsPbX3 (X = Br, I, and Cl) Perovskite Nanocrystals in Polymer Fibers toward Significantly Enhanced Water/Thermal Stabilities, Adv. Opt. Mater. 6 (2018), https://doi.org/10.1002/adom.201800346.

[38] Z. Li, L. Kong, S. Huang, L. Li, Highly Luminescent and Ultrastable CsPbBr 3 Perovskite Quantum Dots Incorporated into a Silica/Alumina Monolith, Angew. Chemie. 129 (2017) 8246–8250, https://doi.org/10.1002/ange.201703264.

[39] H.-C. Wang, S.-Y. Lin, A.-C. Tang, B.P. Singh, H.-C. Tong, C.-Y. Chen, Y.-C. Lee, T.-L. Tsai, R.-S. Liu, Mesoporous Silica Particles Integrated with All-Inorganic CsPbBr 3 Perovskite Quantum-Dot Nanocomposites (MP-PQDs) with High Stability and Wide Color Gamut Used for Backlight Display, Angew. Chemie. 128 (2016), https://doi.org/10.1002/ange.201603698.

[40] T. Leijtens, B. Lauber, G.E. Eperon, S.D. Stranks, H.J. Snaith, The importance of perovskite pore filling in organometal mixed halide sensitized TiO2-based solar cells, J. Phys. Chem. Lett. 5 (2014) 1096–1102, https://doi.org/10.1021/jz500209g.

[41] X. Chen, D. Li, G. Pan, D. Zhou, W. Xu, J. Zhu, H. Wang, C. Chen, H. Song, All-inorganic perovskite quantum dot/TiO2 inverse opal electrode platform: Stable and efficient photoelectrochemical sensing of dopamine under visible irradiation, Nanoscale 10 (2018), https://doi.org/10.1039/c8nr02115e.

[42] T. Xuan, X. Yang, S. Lou, J. Huang, Y. Liu, J. Yu, H. Li, K.L. Wong, C. Wang, J. Wang, Highly stable CsPbBr3 quantum dots coated with alkyl phosphate for white light-emitting diodes, Nanoscale 9 (2017), https://doi.org/10.1039/c7nr04179a.

[43] Y. Gao, N. Guo, B. Gauvreau, M. Rajabian, O. Skorobogata, E. Pone, O. Zabeida, L. Martinu, C. Dubois, M. Skorobogatiy, Consecutive solvent evaporation and co-rolling techniques for polymer multilayer hollow fiber preform fabrication, J. Mater. Res. 21 (2006), https://doi.org/10.1557/jmr.2006.0271.

[44] M. Skorobogatiy, Efficient antiguiding of TE and TM polarizations in low-index core waveguides without the need for an omnidirectional reflector, Opt. Lett. 30 (2005), https://doi.org/10.1364/ol.30.002991.

[45] L. Ramnath, S. DaCosta, S. Akong, H. Hassanali, D. Omonze, J.T. Powers, Fiber optics profiles real-time temperature across horizontal lateral, Oil Gas J 101 (2003).

[46] H. Becker, L.E. Locascio, Polymer microfluidic devices, Talanta 56 (2002), https://doi.org/10.1016/S0039-9140(01)00594-X.

[47] A.C. Henry, T.J. Tutt, M. Galloway, Y.Y. Davidson, C.S. McWhorter, S.A. Soper, R. L. McCarley, Surface modification of poly(methyl methacrylate) used in the fabrication of microanalytical devices, Anal. Chem. 72 (2000), https://doi.org/10.1021/ac000685l.

[48] Y. Zhao, F. Wang, Z.C. Cui, J. Zheng, H.M. Zhang, D.M. Zhang, S.Y. Liu, M.B. Yi, Study of reactive ion etching process to fabricate the PMMA-based polymer waveguide, Microelectronics J 35 (2004), https://doi.org/10.1016/j.mejo.2004.02.005.

[49] B. Ziaie, A. Baldi, M. Lei, Y. Gu, R.A. Siegel, Hard and soft micromachining for BioMEMS: Review of techniques and examples of applications in microfluidics and drug delivery, Adv. Drug Deliv. Rev. 56 (2004), https://doi.org/10.1016/j.addr.2003.09.001.

[50] B.A. Simmons, G.J. McGraw, R.V. Davalos, G.J. Fiechtner, Y. Fintschenko, E. B. Cummings, The development of polymeric devices as dielectrophoretic separators and concentrators, MRS Bull 31 (2006), https://doi.org/10.1557/mrs2006.26.

[51] L. Ravagnan, G. Divitini, S. Rebasti, M. Marelli, P. Piseri, P. Milani, Poly(methyl methacrylate)-palladium clusters nanocomposite formation by supersonic cluster beam deposition: A method for microstructured metallization of polymer surfaces, J. Phys. D. Appl. Phys. 42 (2009), https://doi.org/10.1088/0022-3727/42/8/082002.

[52] S.M.H. Qaid, F.H. Alharbi, I. Bedja, M.K. Nazeeruddin, A.D. Aldwayyan, Reducing Amplified Spontaneous Emission Threshold in CsPbBr3 Quantum Dot Films by Controlling TiO2 Compact Layer, Nanomaterials 10 (2020) 1605, https://doi.org/10.3390/nano10081605.

[53] P. Cottingham, R.L. Brutchey, On the crystal structure of colloidally prepared CsPbBr 3 quantum dots, Chem. Commun. 52 (2016) 5246–5249, https://doi.org/10.1039/C6CC01088A.

[54] X. He, Y. Qiu, S. Yang, Fully-Inorganic Trihalide Perovskite Nanocrystals: A New Research Frontier of Optoelectronic Materials, Adv. Mater. 29 (2017), https://doi.org/10.1002/adma.201700775.

[55] S. Optik, F. Nipis, N. Poli, A. Sio, Optical Properties of Poly(9,9'-di-n-octylfluorenyl-2.7-diyl)/Amorphous SiO2 Nanocomposite Thin Films, Sains Malaysiana 42 (2013) 1151–1157, https://doi.org/10.1063/1.3552594.

[56] C. Wehrenfennig, M. Liu, H.J. Snaith, M.B. Johnston, L.M. Herz, Homogeneous Emission Line Broadening in the Organo Lead Halide Perovskite CH 3 NH 3 PbI 3–x Cl x, J. Phys. Chem. Lett. 5 (2014) 1300–1306. http://pubs.acs.org/doi/abs/10.1021/jz500434p (accessed May 9, 2017).

[57] J.D. Rancourt, Optical Thin Films: User Handbook, SPIE Press, 2009, https://doi.org/10.1117/3.242743.

[58] G. Zhyrair, M. Lenrik, A. Karapet, H. Valeri, A. Eduard, M. Khachatur, Determination of the complete set of optical parameters of micron-sized polycrystalline CH3NH3PbI3-xClx films from the oscillating transmittance and reflectance spectra, Mater. Res. Express. 7 (2019), https://doi.org/10.1088/2053-1591/ab5c46.

[59] Y. Li, W. Yan, Y. Li, S. Wang, W. Wang, Z. Bian, L. Xiao, Q. Gong, S. Wang, W. Wang, Z. Bian, L. Xiao, Q. Gong, S. Wang, W. Wang, Z. Bian, L. Xiao, Direct Observation of Long Electron-Hole Diffusion Distance in CH 3 NH 3 PbI 3 Perovskite Thin Film, Sci. Rep. 5 (2015) 14485, https://doi.org/10.1038/srep14485.

[60] T. Song, Q. Chen, H. Zhou, C. Jiang, H. Wang, M. Yang, Y. Liu, Perovskite solar cells: film formation and properties, J. Mater. Chem. A. 3 (2015) 9032–9050, https://doi.org/10.1039/C4TA05246C.

[61] W.-J. Yin, T. Shi, Y. Yan, Unique properties of halide perovskites as possible origins of the superior solar cell performance, Adv. Mater. 26 (2014) 4653–4658, https://doi.org/10.1002/adma.201306281.

[62] M. Roknuzzaman, C. Zhang, K. Ostrikov, A. Du, H. Wang, L. Wang, T. Tesfamichael, Electronic and optical properties of lead-free hybrid double perovskites for photovoltaic and optoelectronic applications, Sci. Rep. 9 (2019) 718, https://doi.org/10.1038/s41598-018-37132-2.

[63] B.A. Al-Asbahi, S.M.H. Qaid, M. Hezam, I. Bedja, H.M. Ghaithan, A.S. Aldwayyan, Effect of deposition method on the structural and optical properties of CH3NH3PbI3 perovskite thin films, Opt. Mater. (Amst). 103 (2020), https://doi.org/10.1016/j.optmat.2020.109836.

[64] J Tauc, Amorphous and Liquid Semiconductors, Plenum, London, 1974, p. 159, https://books.google.com.sa/books?hl=ar&lr=&id=YKnfBwAAQBAJ&oi=fnd&pg=PA2&dq=Amorphous+and+Liquid+Semiconductors&ots=320BbwpHED&sig=3SKzF2gGi2IhYOZ-ugW5DdICGbQ&redir_esc=y#v=onepage&q=Amorphous and Liquid Semiconductors&f=false (accessed August 6, 2019).

[65] S.M.H. Qaid, M.S. Al Sobaie, M.A. Majeed Khan, I.M. Bedja, F.H. Alharbi, M. K. Nazeeruddin, A.S. Aldwayyan, Band-gap tuning of lead halide perovskite using a single step spin-coating deposition process, Mater. Lett. 1641 (2016) 498–501.

[66] S. Ilican, M. Caglar, Y. Caglar, Determination of the thickness and optical constants of transparent indium-doped ZnO thin films by the envelope method, Mater. Sci. 25 (2007) 709–718.
[67] R. Swanepoel, Determination of the thickness and optical constants of amorphous silicon, J. Phys. E. 16 (2000) 1214–1222.
[68] J.S. Shankar, S. Ashok Kumar, B.K. Periyasamy, S.K. Nayak, Studies on Optical Characteristics of Multicolor Emitting MEH-PPV/ZnO Hybrid Nanocomposite, Polym. - Plast. Technol. Eng. 00 (2018) 1–10, https://doi.org/10.1080/03602559.2018.1466171.
[69] Q. Lin, A. Armin, R. Chandra, R. Nagiri, P.L. Burn, P. Meredith, Electro-optics of perovskite solar cells, Nat. Photonics. 9 (2014) 106–112, https://doi.org/10.1038/nphoton.2014.284.
[70] D.H. Fabini, T. Hogan, H.A. Evans, C.C. Stoumpos, M.G. Kanatzidis, R. Seshadri, Dielectric and Thermodynamic Signatures of Low-Temperature Glassy Dynamics in the Hybrid Perovskites CH3NH3PbI3 and HC(NH2)2PbI3, 7 (2016). doi:10.1021/acs.jpclett.5b02821.
[71] P. Löper, M. Stuckelberger, B. Niesen, J. Werner, M. Filipič, S.-J. Moon, J.-H. Yum, M. Topič, S. De Wolf, C. Ballif, Complex Refractive Index Spectra of CH 3 NH 3 PbI 3 Perovskite Thin Films Determined by Spectroscopic Ellipsometry and Spectrophotometry, J. Phys. Chem. Lett. 6 (2015) 66–71, https://doi.org/10.1021/jz502471h.
[72] X. Ziang, L. Shifeng, Q. Laixiang, P. Shuping, W. Wei, Y. Yu, Y. Li, C. Zhijian, W. Shufeng, D. Honglin, Y. Minghui, G.G. Qin, Refractive index and extinction coefficient of CH3NH3PbI3 studied by spectroscopic ellipsometry, Opt. Mater. Express. 5 (2014) 29, https://doi.org/10.1364/OME.5.000029.
[73] A Yang, M Bai, X Bao, J Wang, W Zhang, Investigation of Optical and Dielectric Constants of Organic-Inorganic CH3NH3PbI3 Perovskite Thin Films, J. Nanomed. Nanotechnol. 07 (2016), https://doi.org/10.4172/2157-7439.1000407.
[74] T. Arumanayagam, P. Murugakoothan, Optical Conductivity and Dielectric Response of an Organic Aminopyridine NLO Single Crystal, J. Miner. Mater. Charact. Eng. 10 (2011) 1225–1231.